ADVANCED INTELLIGENT SYSTEMS
Open Access
www.advintellsyst.com

A Bioinspired Shape Memory Alloy Based Soft Robotic System for Deep-Sea Exploration

Yi Xu, Jiangshan Zhuo, Mingyu Fan, Xinge Li, Xunuo Cao, Dongrui Ruan, Hejinsheng Cao, Fanghao Zhou, Tuck-Whye Wong, and Tiefeng Li*

Developing robots integrating sensors, actuators, and computational capabilities for deep-sea exploration is challenging. Nature often offers innovative solutions to complex problems, and in this context, inspiration is drawn from the remarkable abilities of deep-sea snails, specifically their unique tentacles, often referred to as "eyestalks" due to the presence of an eye at their tip. Herein, "DeepStalk," a soft robot designed for deep-sea exploration, is introduced, utilizing three shape memory alloys (SMAs) springs that mimic the three tentacle flexor muscles of deep-sea snails. Overall, DeepStalk incorporates sensory, actuation, and control modules for operation under high hydrostatic pressure. To achieve precise control of its orientation in 3D space, a simple and reliable vector-PID controller is developed. Remarkably, the robot successfully maintains its desired bending attitude even at 30 MPa hydrostatic pressure, achieved through the Joule heating of SMA springs. Furthermore, DeepStalk demonstrates the capability to track moving objects underwater, showcasing its potential application in challenging environments at depths of up to 20 MPa. This marks the first attempt for soft robots to integrate sensor, actuator, and control modules capable of complex tasks under high hydrostatic pressure. This innovative research advances integrated soft robotic systems for deep-sea exploration field.

1. Introduction

Rigid-bodied robots are widely employed in task execution for their inherent efficiency. However, rigid-bodied robots are limited in compliance and adaptability due to their inflexible links and joints. In contrast to rigid structures, soft robots offer numerous advantages, including high adaptability, biocompatibility, and multifunctionality.[1–4] A class of soft robots used underwater is developed by marine organisms.[5] Examples include a soft robot inspired in morphology and behavior by jellyfish,[6] a soft robot arm inspired by the octopus,[7] fast-moving soft electronic fish,[8] and more. However, due to the extremely high pressure, the abyssal zone of the ocean is the least explored place on Earth.[9] The mechatronic systems of traditional robots need to be protected by rigid pressure vessels if operating in the deep sea. In contrast, soft robots hold the potential to address the challenges inherent to deep-sea exploration.[10] Inspired by snailfish, Li et al.[11] developed a self-powered soft robotic fish that actuated successfully in the Mariana Trench. Existing soft robots or actuators capable of working in the deep sea are limited by the extremely high hydrostatic pressure. Most of them exhibit a simple structure executing only a single function, either actuation or sensing, which is incapable of more complex tasks.[9,12–14]

As a typical mollusk, sea snails are a varied group of gastropods that inhabit every ocean in the world. A snail orients itself in its surroundings using tentacles. The tentacular sensory organs of the posterior head tentacles take a leading role in the orientation of snails in space. The posterior tentacle is also known as the eyestalk, on the tips of which the eyes of the snails are located.[15] For instance, Queen Conch is a type of sea snail with long eyestalks (**Figure 1**a). An eyestalk displays different types of motor patterns, such as scanning the environment in three dimensions,

Y. Xu, X. Li, X. Cao, D. Ruan, F. Zhou, T. Li
State Key Laboratory of Fluid Power and Mechatronic Systems
Zhejiang University
Hangzhou 310027, China
E-mail: zhoufanghao@zju.edu.cn

The ORCID identification number(s) for the author(s) of this article can be found under https://doi.org/10.1002/aisy.202300699.

DOI: 10.1002/aisy.202300699

Y. Xu, J. Zhuo, X. Li, X. Cao, D. Ruan, F. Zhou, T.-W. Wong, T. Li
Department of Engineering Mechanics
Zhejiang University
Hangzhou 310027, China

M. Fan
School of Design
Politecnico di Milano
20133 Milano, Italy

H. Cao
Shaoxing Haivoo Power Supply Technology Co., Ltd
Shengzhou 312400, Shaoxing, China

T.-W. Wong
Department of Biomedical Engineering and Health Sciences
Universiti Teknologi Malaysia
Skudai 81310, Malaysia

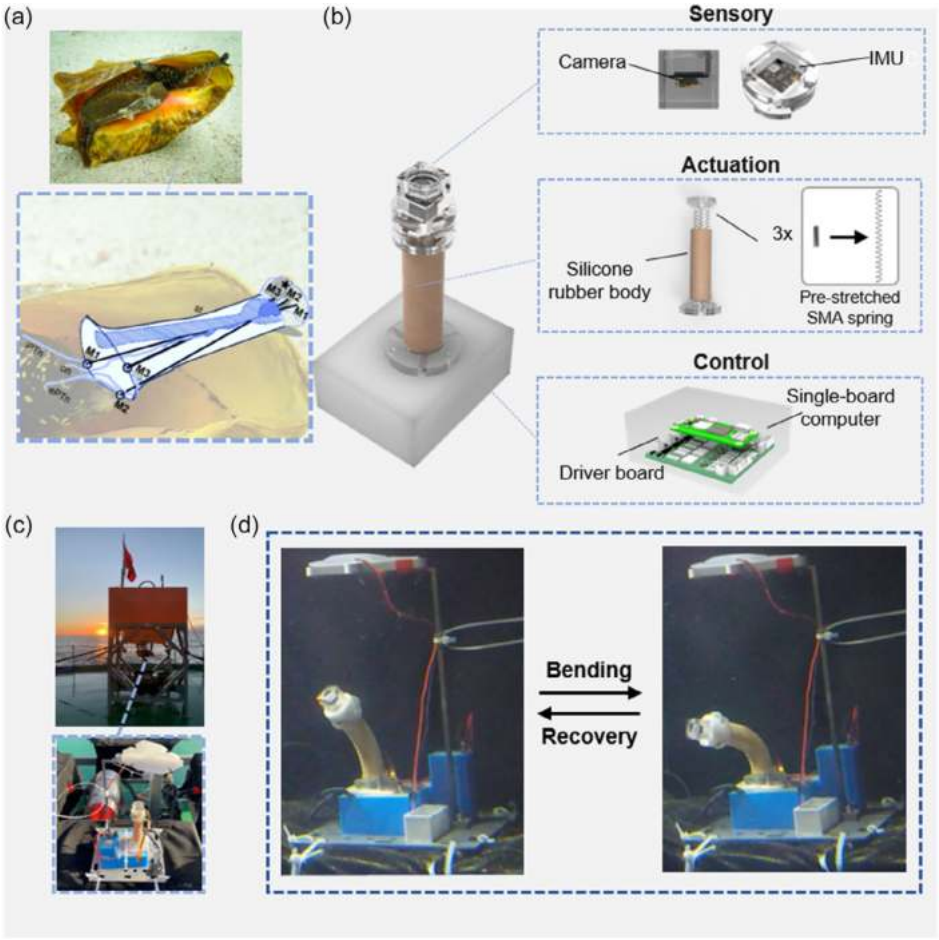

Figure 1. Design of the "DeepStalk" inspired by deep-sea snails' eyestalk and deep-sea field test. a) Sea snail Queen Conch (Daniel Neal from Sacramento, CA, US, CC BY 2.0, via Wikimedia Commons) and anatomy of snail eyestalk (tentacle). The eyes of the snails are located on the tips of the tentacles. Three tentacle flexor muscles also called string muscles (M1, M2, and M3) are responsible for different types of motor patterns. b) Schematic of the "DeepStalk." Inspired by the eyestalk, the design of DeepStalk consists of a sensor, actuation, and control module. c) In a field test in the South China Sea (18.14°N, 111.03°E), the soft robot was carried by a deep-sea lander. d) This robot completed the process of bending and recovering movements at the bottom of the sea.

quivering, and twitching.[16] As shown in Figure 1a, three tentacle flexor muscles also called string muscles (M1, M2, and M3) are responsible for these motor patterns by contraction.[17] M1, M2, and M3 are innervated by the internal peritentacular nerves and two external peritentacular nerves.[18] Snails' eyestalks are highly flexible and can move in different directions, which allows them to have a wide field of vision. This helps the snails detect predators and potential food sources from a distance. Snails in the deep sea have evolved to withstand high pressure and survive in the harsh conditions of the abyssal depths.

In this article, we present a low-cost and modularized bioinspired soft eyestalk robot, DeepStalk, designed for deployment in the deep sea. Experiments demonstrate that DeepStalk exhibits a remarkable ability to bend to the anticipated orientation at maximum hydrostatic pressure of 30 MPa. In addition, object-tracking experiments have been conducted to test the potential application of DeepStalk for deep-sea exploration.

2. Design and Achievement

We propose a soft robot inspired by deep-sea snails' eyestalk—DeepStalk. It consists of a sensor, actuation, and control module (Figure 1b). The sensor module, analogous to the sensory organ found in the eyestalk, encompasses an inertial measurement unit (IMU) in conjunction with a miniature camera (RaspberryPi Zero OV5647). The IMU module is reconfigured and packaged to be pressure-tolerant and capable of functioning effectively even under demanding conditions of 30 MPa pressure. The miniature camera is encased in a 3D-printed protective housing to enable its functionality at the abyssal depths of the ocean, a design taking reference from the DEEPi system.[19] The camera protective housing is made of epoxy resin and the overall size is $2 \times 2 \times 2\ cm^3$. The actuation module consists of top and bottom plates, three shape-memory alloy (SMA) springs, and a silicone rubber body. SMA springs have served as actuators in the field of soft robotics for a long time.[20–22] SMAs are efficient and reliable

in challenging underwater environments because of their corrosion resistance, lightweight design, high power density, and low noise.[23] The sensor module acts as the load for the actuation module, aiming to achieve the maximum possible working space and return to the initial position in the free state. The silicone rubber body is made from silicone gel (Shore A hardness ≈5) with a length of 80 mm and a cross-sectional diameter of 24 mm. The three SMA springs (BH-QS06, Baohong), which act as three tentacle flexor muscles, are located 120° apart around the central axis of the silicone rubber body. The spring diameter and wire diameter are 4 and 0.5 mm, respectively. The SMA springs are prestretched three times with a 4 mm pitch to acquire the deformation ability. The top and bottom plates are used to connect and fix the SMA springs. The shape-memory effect is a unique property of SMAs that allows them to remember their original shape and recover it when subjected to certain external stimuli, such as heat or stress.[23] When one of the springs placed in the silicone rubber body and fixed by top and bottom plates is heated, it will distribute a force of contraction and make the body bend toward the spring's orientation. Analogously, in scenarios involving the heating of dual springs, the SMA-driven actuator will bend to the orientation between the two springs. Finally, the control module comprises a single-board computer (RaspberryPi Zero2W) and a self-designed SMA driver board. The outputs of the driver board serve three purposes: to actuate the SMA springs, to supply power to the IMU, and to supply power to the single-board computer. The control module is encapsulated in a polymeric matrix (Dragon Skin 20). Certain electronic components are specifically modified to withstand high hydrostatic pressure.[11] The control module is enhanced to be pressure-tolerant so that it can withstand underwater depths of up to 3000 m.

DeepStalk was actuated successfully in a field test in the South China Sea (18.14°N, 111.03°E). In the test, DeepStalk was carried by a deep-sea lander (Figure 1c) to a depth of 201 m. The robot was self-powered by an onboard lithium-ion battery (1300 mAh) and bent up to 70° (Figure 1d). While the robot was bending, the miniature camera kept observing the surrounding environment. Details of the field experiments can be found in Supporting Information (Movie S1 and S2, Supporting Information).

3. System Architecture

Figure 2b depicts the system architecture of DeepStalk, with a DC power source and a host computer for data transmission. The entire system is powered by the DC power source with a voltage of 12 V. The SMA driver board communicates with other devices via serial ports, and the camera is linked to the single-board computer via a flexible flat cable, enabling the transmission of video signals. The IMU transmits the attitude data to the SMA driver board. The single-board computer processes the video from the camera and sends target position data to the SMA driver board.

DeepStalk possesses two distinct control modes: attitude control and object tracking. The switch between the control modes can be achieved by the host computer. In the attitude control mode, which involves the IMU and driver board, we acquire the Euler angle (β_t, α_t) pertaining to the eyestalk end through the employment of the IMU as a feedback parameter. The Euler angle information is then sent to the SMA driver board where it is processed via a vector-PID controller. Subsequently, we regulate the output current $(I^1_{out}, I^2_{out}, I^3_{out})$ of the SMA driver, which, in turn, governs the behavior of the three SMA springs. This process is directed by a closed-loop control algorithm. In the object tracking mode, which involves the camera, the single-board computer, and the driver board, we obtain the object position (x_t, y_t) by the single-board computer and the camera module. Similar to the attitude control mode, the SMA driver applies a control current which is obtained via a closed-loop controller to regulate the eyestalk's attitude and track the object. The two control modes will be discussed in detail later.

4. Kinematic Model

We can obtain the relationship between the Euler angles and the joint angles of the system by modeling the kinematics of the structure, which facilitates the feedback control of the actuator.

As shown in Figure 2a, the configuration of the eyestalk is determined by the joint angles including the deflection angle α and the bending angle β. Coordinate systems O_0 and O_1 are set up at the bottom and the top of the configuration. The bending angle β describes the bending deformation of the actuator, while the deflection angle α describes the bending direction of the actuator.

Two assumptions are made to build the kinematic model: 1) the central axis of the bending cylinder is an arc; 2) the bending curvature along the central axis is constant.

According to the spatial robot kinematics of continuum-style robots proposed by Walker,[24] the transformation matrix from the initial configuration O_0 to the terminal configuration O_1, noted as T^1_0, can be expressed by the joint angles α and β as follows

$$T^1_0 = \mathrm{rot}(Z,\alpha)\mathrm{rot}\left(Y,\tfrac{\beta}{2}\right)\mathrm{trans}(0,0,L)\mathrm{rot}\left(Y,\tfrac{\beta}{2}\right)\mathrm{rot}(Z,-\alpha) \quad (1)$$

where L is the chord length of the eyestalk's central axis.

Regardless of the spatial position, let R^1_0 represent the rotation matrix from the initial configuration O_0 to the terminal configuration O_1.

The terminal attitude of the eyestalk can also be described by the Euler angles. The rotation matrix of O_1 with respect to the earth coordinate[25] is denoted as R^1_E, while for O_0 the rotation matrix is R^0_E. Therefore, the rotation matrix of O_1 with respect to O_0 is

$$R^1_0 = (R^0_E)^{-1} \times R^1_E = (R^0_E)^T \times R^1_E \quad (2)$$

Thus, we can get the deflection angle α and the bending angle β represented by Euler angles (the results are shown in Section S1, Supporting Information).

5. Control Scheme

To govern the eyestalk to attain a target attitude, we need to control the current applied to three SMA springs. Thus, we develop a simple and reliable vector-PID controller for closed-loop control, inspired by field-oriented control, which is commonly used in

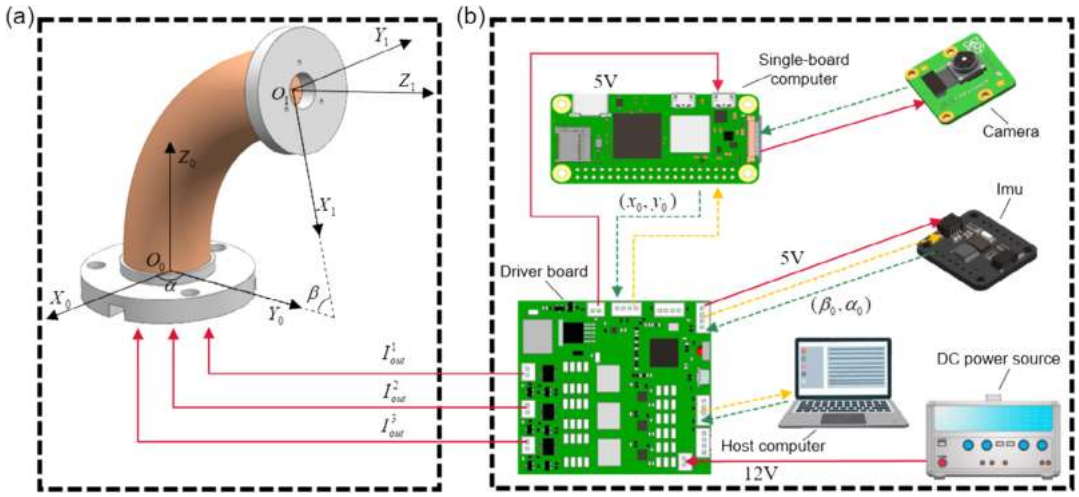

Figure 2. Kinematic description and system architecture. a) The configuration of the eyestalk is determined by the deflection angle α and the bending angle β. Coordinate systems O_0 and $_1$ are set up at the bottom and the top of the configuration. The bending angle β describes the bending deformation of the actuator, while the deflection angle α describes the bending direction of the actuator. b) System architecture of the DeepStalk (red solid lines represent supply current; dashed lines represent signals, where yellow indicates transmit and green indicates receive).

electric motor control.[26] The primary objective of this controller is to control the attitude of DeepStalk, and to control the camera affixed at its terminus to track moving objects. The flowchart of the controller is shown in **Figure 3**a, which contains three parts: attitude control, PID control, and object tracking. Overall, the output of the attitude control or object tracking serves as the input of the PID control procedure to generate the required current. Compared to existing controllers for similar SMA-driven actuators,[27] the vector-PID controller contains only one PID controller channel and the control algorithm is simpler. In such extreme environments as the deep sea, the performance of electronic devices is typically unstable. Therefore, simple controllers often guarantee more reliability.

5.1. Attitude Control

In this mode, DeepStalk is directly controlled to track the target joint angle (β_t, α_t). The current joint angle (β, α) can be calculated using inverse kinematics, which converts from the Euler angle acquired from IMU. The detailed algorithms have been described in the kinematic model.

5.1.1. Vectorization

The two joint angles are converted into a vector in this step. As discussed in the previous section, the deformed shape of the eyestalk is defined by the bending angle β and the deflection angle α. Next, the two joint angles combine into a vector. The bending angle denotes the orientation of the vector, and the deflection angle denotes the amplitude of the vector. The vector is shown in Figure 3b(i). Let (β_0, α_0) denote the initial attitude and (β_t, α_t) denote the target attitude. Then, we can obtain the error vector $(\beta_{err}, \alpha_{err})$, which is the input to the PID controller, by vector subtraction as shown in Figure 3b(ii).

5.2. Object Tracking

The miniature camera is "the eye of the robot." It is used for not only capturing images and videos but also for recognizing target objects. Thus, the manipulation of the eyestalk allows for the tracking of the target objects. Namely, the object track controller introduced here maintains the target object in the center of the camera view. It is similar in principle to attitude control.

5.2.1. Object Detection

The position of the target object in the camera view is obtained in this step. As illustrated in Figure 3c, we take the lower left corner of the camera view as the origin to establish a rectangular coordinate system. The center of the camera view is denoted as the reference point (x_{ref}, y_{ref}), and the center of the target object's outer circle is the current point (x_t, y_t). Various algorithms are available for detecting the target object's current point. To speed up the computation, we employ a color recognition algorithm based on OpenCV. After obtaining the current point, the error vector (x_{err}, y_{err}) can be acquired as the vector extending from the reference point to the current point (see Figure 3c).

5.3. PID Control

This module is responsible for receiving the output of the above two modules and controlling the current applied to the SMA springs.

5.3.1. Mode Switch

As the other two modules represent different control modes, one of them is selected as an input for the PID control.

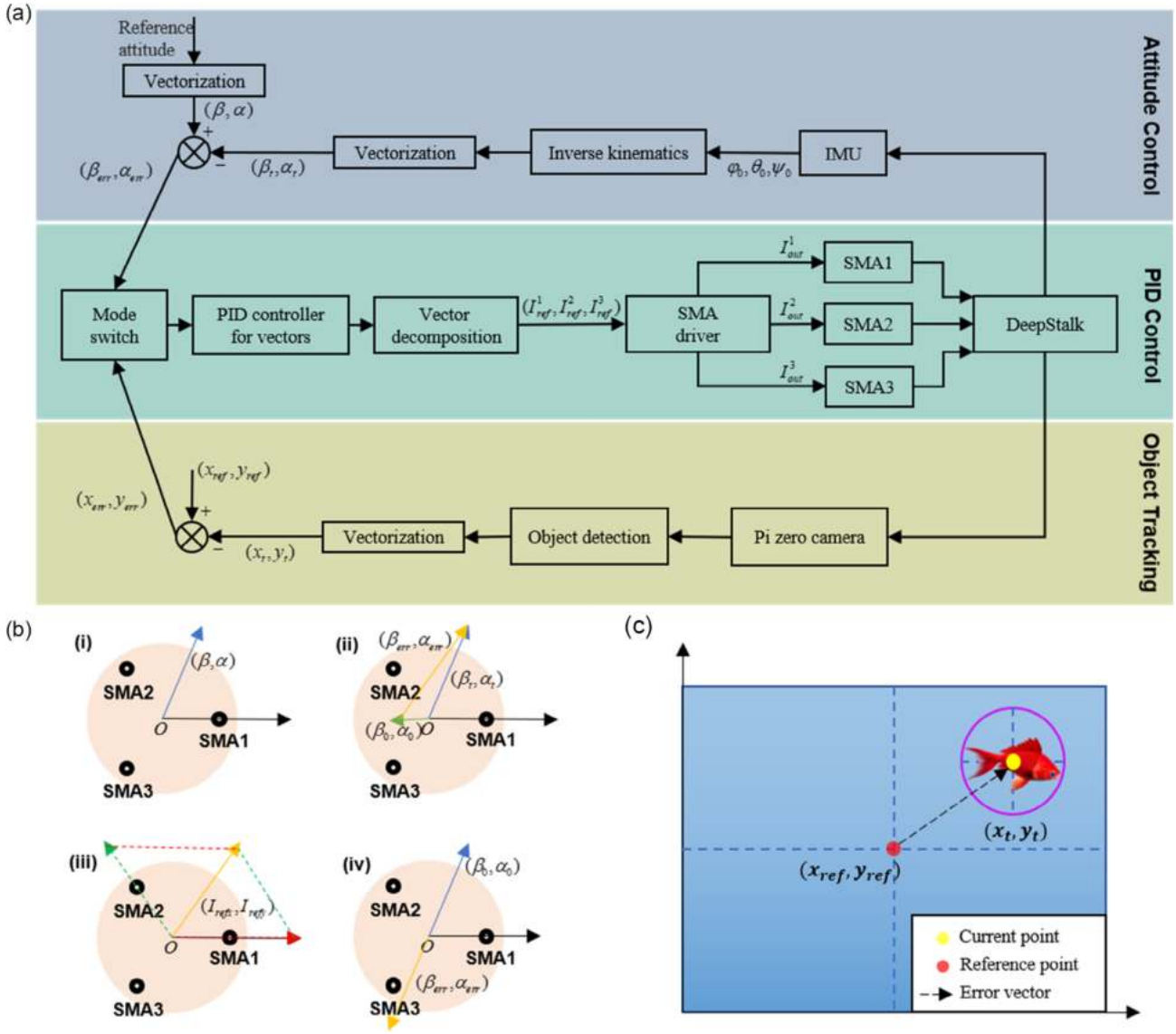

Figure 3. Control scheme of the DeepStalk. a) The flowchart of vector-PID controller for attitude control and object tracking control. b) Graphical representation of vectors in attitude control: i) vectorization, ii) the error vector as the input to the PID controller, iii) vector decomposition, and iv) cooling progress. c) The diagrams of object detection. The reference point is obtained in this step and thus we can get the error vector for PID controller.

5.3.2. PID Controller for Vectors

In the attitude control mode, $(\beta_{\text{err}}, \alpha_{\text{err}})$ is the error vector (input) for the controller.

In the rectangular coordinate system, $(\beta_{\text{err}}, \alpha_{\text{err}})$ can be described as

$$(\beta_{\text{err}}\cos\alpha_{\text{err}}, \beta_{\text{err}}\sin\alpha_{\text{err}}) = (\beta_{\text{t}}\cos\alpha_{\text{t}}, \beta_{\text{t}}\sin\alpha_{\text{t}}) - (\beta_0\cos\alpha_0, \beta_0\sin\alpha_0) \tag{3}$$

Denoting the error vector as $\overrightarrow{e_{\text{a}}}(t)$, $e_{\text{a}x}(t)$ and $e_{\text{a}y}(t)$ are its components on the x and y axes, respectively.

$$\vec{e}_{\text{a}}(t) = (e_{\text{a}x}(t), e_y(t)) = (\beta_{\text{err}}\cos\alpha_{\text{err}}, \beta_{\text{err}}\sin\alpha_{\text{err}}) \tag{4}$$

Denoting the output of the PID controller as $\vec{I}_{\text{ref}}$, $I_{\text{ref}x}$ and $I_{\text{ref}y}$ are its components on the x and y axes, respectively.

$$\vec{I}_{\text{ref}} = (I_{\text{ref}x}, I_{\text{ref}y}) \tag{5}$$

The input and output of the PID controller are related by the following equations

$$I_{\text{ref}x} = K_{ap}e_{\text{a}x}(t) + K_{\text{a}i}\int_0^t e_{\text{a}x}(t)\text{d}t + K_{ad}\frac{de_{\text{a}x}(t)}{\text{d}t} \tag{6}$$

$$I_{\text{ref}y} = K_{ap}e_{\text{a}y}(t) + K_{\text{a}i}\int_0^t e_{\text{a}y}(t)\text{d}t + K_{ad}\frac{de_{\text{a}y}(t)}{\text{d}t} \tag{7}$$

where K_{ap}, $K_{\text{a}i}$, and K_{ad} are proportional, integral, and differential coefficients of the attitude control, respectively.

In the object track mode, (x_{err}, y_{err}) is the error vector (input) of the PID controller.

And the output $(I^c_{ref\,x}, I^c_{ref\,y})$ is

$$I^c_{ref\,x} = K_{op} x_{err}(t) + K_{oi} \int_0^t x_{err}(t)dt + K_{od} \frac{dx_{err}(t)}{dt} \quad (8)$$

$$I^c_{ref\,y} = K_{op} y_{err}(t) + K_{oi} \int_0^t y_{err}(t)dt + K_{od} \frac{dy_{err}(t)}{dt} \quad (9)$$

where K_{op}, K_{oi}, and K_{od} are the controller parameters of object tracking, x_{err} is the error in the x direction calculated by $x_{err}(t) = x_t - x_{ref}$, and y_{err} is the error in the y direction calculated by $y_{err}(t) = y_t - y_{ref}$.

5.3.3. Vector Decomposition

The reference current applied to each SMA spring is computed in this step. Three SMA springs are positioned 120° apart around the central axis of the silicone rubber body. Nevertheless, it is not necessary to heat all of them. By heating one or a pair of SMA springs, the eyestalk can bend in various directions. For instance, when both SMA1 and SMA2 are heated, the eyestalk will bend within the range of 0°–120°. The three SMA springs divide the bending direction into three parts (0°–120°, 120°–240°, and 240°–360°). Therefore, we should determine which part $\vec{I}_{ref}$ belongs to, which is straightforward because $I_{ref\,x}$ and $I_{ref\,y}$ have been identified in the last step. As shown in Figure 3b(iii), the current applied to each spring can be derived through vector decomposition (the results are shown in Section S2, Supporting Information).

5.3.4. SMA Driver

The SMA driver board provides the controlled current, regulated by a closed-loop controller, to actuate the SMA springs.

We have completed the design of the vector-PID controller which is suitable for both attitude control and object track modes. The controller exhibits a simple and symmetrical design, enabling a fast processing speed in the embedded development boards.

SMA actuators usually exhibit certain constraints. When the SMA springs are cooled, they will retract and the eyestalk will return to its original attitude gradually. The primary issue with bandwidth limitation lies in the slow cooling process, where the rate of heat energy removal is constrained by the mechanisms of heat conduction and convection.[23] Thus, active cooling is typically demonstrated to increase the bandwidth.[27] However, the addition of other devices will complicate the system. Instead, our control method can help accelerate the recovery process without adding other devices. To make DeepStalk return to its original attitude faster than natural heat dissipation, one or two SMA springs are heated inducing a return to the original attitude. The control strategy is depicted in Figure 3b(iv) where the reference attitude in this case is $(0, 0)$. Accordingly, the error vector is opposite to the initial vector (β_0, α_0). As a result, the eyestalk will bend in the opposite direction. Finally, the eyestalk will recover to its original shape when the error vector reaches $(0, 0)$.

6. Attitude Control Experiments

Bending in different directions is the basic ability of DeepStalk and the entire system is designed to be applied in the deep sea. Therefore, experiments are set up, as depicted in Figure S1a, Supporting Information, for validation. To simulate the deep-sea environment, the robot is attached to the bottom of a pressure chamber, where the pressure is elevated by a pump and monitored by a pressure console (Figure S1b, Supporting Information).

6.1. Control of the Deflection Angle

We assess DeepStalk's capability of bending to fixed positions. We set up four target attitudes with deflection angles of 80°, 170°, 260°, and 350°, respectively, along with fixed bending angles. DeepStalk starts with an initial attitude, moves to the target attitude, and then returns to the initial attitude before moving to the next target. During these movements, the IMU records the actual deflection angle and actual bending angle. The error of the deflection angle is quantified as the absolute value of the difference between the actual deflection angle and the target deflection angle. So is the error of the bending angle. In the phase of moving to the target attitude, when both the deflection angle error and the bending angle error are less than 1°, we define that the robot has reached the target attitude, and it will return. In the phase of returning to the initial attitude, when both the deflection angle error and bending angle error are less than 4°, we define that the robot has reached the initial attitude, and it will move to the next target attitude. The experiment is conducted under pressure of 0 and 30 MPa and the results are shown in **Figure 4**d,e. The additional snapshots of the experiment conducted under 0 MPa are shown in Figure S2, Supporting Information.

The results demonstrate that DeepStalk can reach the four target attitudes using the vector-PID controller. The deviation of both the deflection angle and bending angle is 1°. Besides, the system and the controller can both work under high hydrostatic pressure. It is worth noting that the deflection angle exhibits significant fluctuations when DeepStalk returns to its initial orientation. This is because the deflection angle is sensitive when the bending angle is close to zero.[28] A comparison of the results in Figure 4d,e shows that at least one output current has reached the current limit almost throughout the experiment under 30 MPa. This implies that a greater current is required to actuate the robot when subjected to increased hydrostatic pressure. That is to say, more contraction force distributed by SMA springs is needed to bend the robot. One possible reason is that the Young's modulus of silicone increases with the pressure.[29,30]

6.2. Control of the Bending Angle

We assess DeepStalk's capability of bending to a stepped target attitude. The target bending angle is set from 0° to 50°, and then back to 0°, with a step of 10°. Each step has a duration of 60 s. The target deflection angle is fixed at 0°. The experiment is conducted under pressure of 0 and 30 MPa. Some snapshots under 0 MPa are shown in Figure 4a. The whole process consists of a bending process and a recovery process. The SMA1 functions as the primary actuating spring in the bending process. The SMA2 and SMA3 collaborate to maintain the deflection angle at 0°. On the contrary, the SMA2 and SMA3 are the primary actuating springs in the

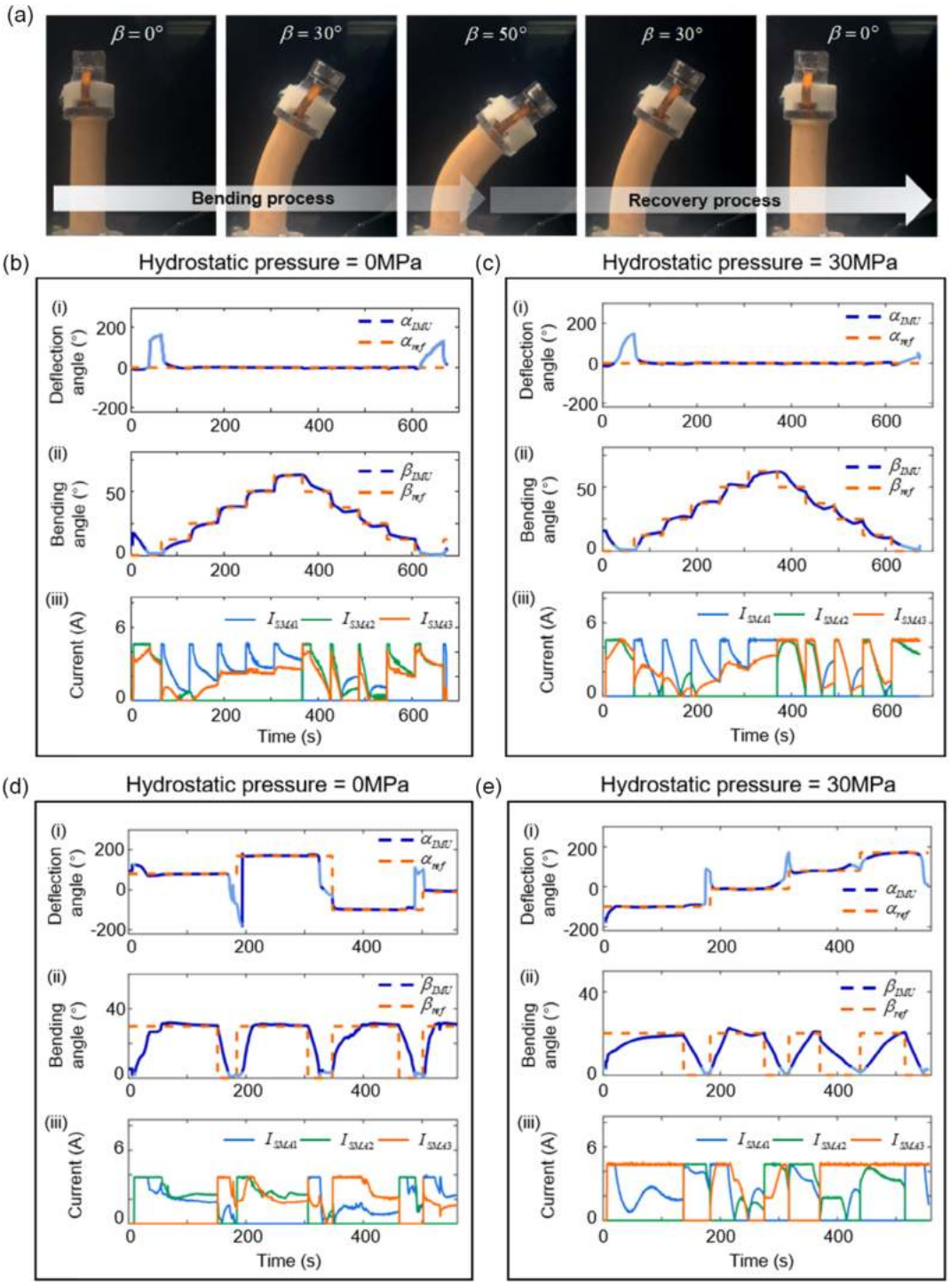

Figure 4. Attitude control experiment. a) The experimental progress of controlling the bending angle. Snapshots of the DeepStalk in some target attitude. b) Experimental result of control of the bending angle under pressure of 0 MPa. Experimental data for i) deflection angle, ii) bending angle, and iii) current. c) Experimental result of control of the bending angle under pressure of 30 MPa. Experimental data for i) deflection angle, ii) bending angle, and iii) current. d) Experimental result of control of the deflection angle under pressure of 0 MPa. Experimental data for i) deflection angle, ii) bending angle, and iii) current. e) Experimental result of control of the deflection angle under pressure of 30 MPa. Experimental data for i) deflection angle, ii) bending angle, and iii) current.

recovery process. The SMA1 helps when overshooting. Therefore, our robot bends in a fixed direction but all the springs are involved. The experiment results are shown in Figure 4b,c. We can see that DeepStalk reaches each bending angle step and maintains the deflection angle constant under 0 and 30 MPa.

6.3. Dynamic Control

We also conduct experiments to evaluate DeepStalk's capability of tracking a preset trajectory. The trajectory set is a circle (the reference deflection angle increases from 80° to 440° at a uniform rate in 360 s with the reference bending angle maintained at 20°). The experiments are conducted under 0 and 30 MPa. The experiment under 0 MPa is recorded in Movie S3, Supporting Information. From Figure S3a,b, Supporting Information, we can see that the actual track is almost consistent with the reference track under 0 and 30 MPa. There are several obvious fluctuations in the process of bending angle control that occur during the switch of the heating SMA springs. The abrupt contraction of another

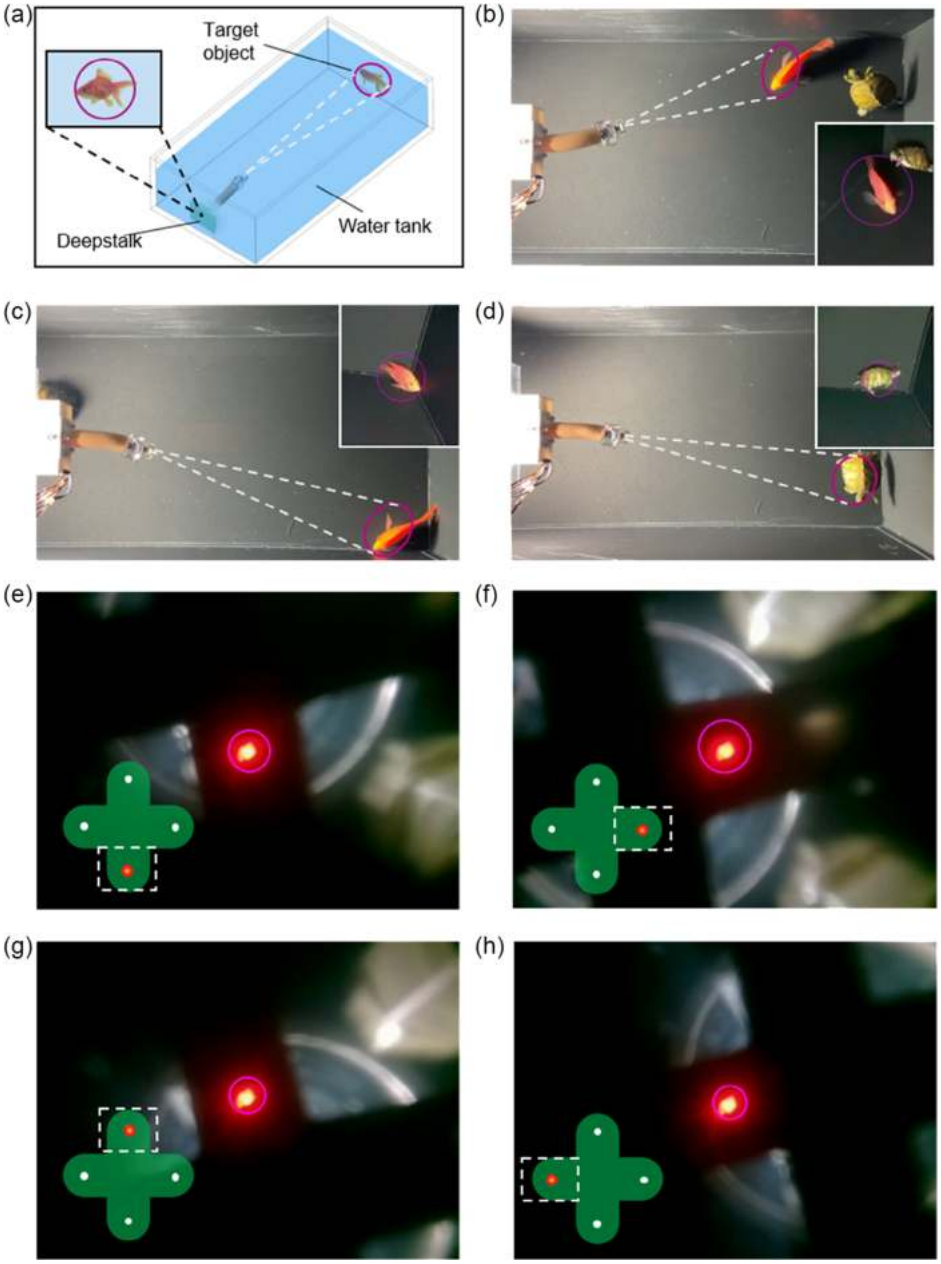

Figure 5. Object tracking experiments. a) Experimental setup of underwater moving target tracking. The experiment is conducted in a water tank. DeepStalk is fixed on the wall of the water tank. b–d) Snapshot when capturing the target object. Both the view of the robot's own camera and the view of the camera on top of the experimental setup are shown. e–h) Experimental results of target tracking under high pressure. Snapshots when catching each LED (lower left diagrams represent the sequence of LEDs and the dotted white boxes represent the camera view).

SMA spring, which has not been heated before, causes the system to fluctuate.

7. Object Tracking Experiments

7.1. Experimental Setup of Object Tracking

Two experiments are conducted to test DeepStalk's capability of object tracking and system reliability under high hydrostatic pressure. The first experiment aims at underwater moving target tracking, while the other aims at target tracking under high pressure.

7.1.1. Underwater Moving Target Tracking

The experiment is conducted in a water tank (**Figure 5**a) with DeepStalk fixed on the wall of the water tank. Two species, *Amphilophus* (a kind of fish) and *Trachemys scripta* (a kind of turtle), are set as the target objects. These species are distinguished by their distinct colors, which serve as the primary feature for target identification.

7.1.2. Target Tracking Under High Pressure

This experimental setup is similar to that of attitude control. The difference is that a set of LEDs (a total of four) is placed in the pressure chamber as the target object. The four LEDs are mounted on a bracket and powered, in turn, by a circuit board. Figure S1c, Supporting Information, shows the position of the four LEDs.

7.2. Underwater Moving Target Tracking

After characterizing DeepStalk's attitude control performance, we proceed to investigate its real-world applications. We demonstrate DeepStalk's capabilities in identifying and tracking underwater objects, with specific reference to a fish and a turtle, representing fast-moving and slow-moving objects, respectively. Snapshots capturing the target objects are shown in Figure 5b–d. Both the view of the robot's internal camera and the view of the top observer camera are displayed. The relevant video can be found in Movie S4, Supporting Information. Notably, DeepStalk can track the fish and the turtle smoothly, even when they are in the camera view at the same time.

7.3. Target Tracking Under High Pressure

The deep sea environment is the primary field of operation for our robot. However, it is difficult to conduct the last experiment (underwater moving target tracking) under high pressure. Therefore, LEDs replace marine creatures as our tracking targets. We set up four red LEDs, with only one lighting up at a time and switching to the next every 20 s. Our task is to control the posture of the robot so that the LEDs are in the center of the robot's field of vision. The experiment is conducted at 20 MPa. The process of target tracking is recorded in Movie S5, Supporting Information and the experiment results are shown in Figure 5e–h. During the lighting period of each LED, DeepStalk catches up with the LED and keeps it in the center of the vision successfully. This proves that our robot has the potential to track moving objects in the deep sea. Meanwhile, overshooting and vibrations during the periods of certain LEDs are observed because the mechanical properties of the three SMA springs vary, but the PID controller parameters remain consistent for each spring.

8. Conclusion

In conclusion, this article presents DeepStalk, a breakthrough soft robot inspired by eyestalks, powered by SMA springs, and utilizing a vector-PID controller for precise attitude control or object tracking. Notably, we introduce innovative strategies to address key challenges in underwater robotics. Our robotic design circumvents the necessity of employing rigid vessels to shield against extreme pressure. Moreover, the utilization of SMA springs enhances the overall structural compactness, ensuring efficient performance. Additionally, we implement a vector-PID controller for closed-loop control that optimizes SMA actuation, avoiding the complex electro-thermo-mechanical dynamic of SMA. These advancements significantly improve the robot's performance and control accuracy.

Our robot is an attempt to integrate sensing, actuating, and control systems in a soft device that can perform complex tasks in the deep sea. DeepStalk demonstrates remarkable two-degree-of-freedom bending capabilities and is equipped with an IMU and a miniature camera, making it suitable for deep-sea exploration at depths of up to 2000 m. Our experiments validate its precise attitude control, even under the extreme hydrostatic pressure of 30 MPa. These innovations mark a significant step forward in integrated soft robotics for deep-sea exploration, offering the potential to revolutionize how we navigate and study the ocean's abyssal depths. The strategies presented in this work pave the way for more efficient, adaptable, and capable robots in this challenging domain, opening new horizons for underwater exploration and research. However, our robot has certain limitations, including slow response speed and a maximum depth limit of 3,000 meters. Future work will involve optimizing the design of the actuation module and the control scheme to achieve greater flexibility and faster deformation. Additionally, efforts will be made to enhance the pressure-tolerant performance of electronic devices.

Supporting Information

Supporting Information is available from the Wiley Online Library or from the author.

Acknowledgements

The authors would like to thank the support from the following: the National Natural Science Foundation of China (grant nos. T2125009, T2293722, and 92048302); the National Postdoctoral Program for Innovative Talents (grant no. BX20220272); the "Pioneer" R&D Program of Zhejiang (grant no. 2023C03007); and the Laoshan Laboratory (grant no. LSKJ202205300). The mechatronic equipment was supported by the Shaoxing Haivoo Power Supply Technology.

Conflict of Interest

The authors declare no conflict of interest.

Data Availability Statement

The data that support the findings of this study are available from the corresponding author upon reasonable request.

Keywords

bioinspired robotics, deep-sea exploration, shape-memory alloys

Received: October 30, 2023
Revised: January 21, 2024
Published online: February 17, 2024

[1] J. Fang, Y. Zhuang, K. Liu, Z. Chen, Z. Liu, T. Kong, J. Xu, C. Qi, *Adv. Sci.* **2022**, *9*, 2104347.
[2] M. Cianchetti, C. Laschi, A. Menciassi, P. Dario, *Nat. Rev. Mater.* **2018**, *3*, 143.
[3] S. I. Rich, R. J. Wood, C. Majidi, *Nat. Electron.* **2018**, *1*, 102.
[4] H. Shen, *Nature* **2016**, *530*, 24.
[5] C. Laschi, M. Calisti, *Nature* **2021**, *591*, 35.
[6] C. Cruz, S. Terrile, A. Barrientos, *Appl. Sci.* **2020**, *10*, 7160.
[7] C. Laschi, M. Cianchetti, B. Mazzolai, L. Margheri, M. Follador, P. Dario, *Adv. Robot.* **2012**, *26*, 709.
[8] T. Li, G. Li, Y. Liang, T. Cheng, J. Dai, X. Yang, B. Liu, Z. Zeng, Z. Huang, Y. Luo, T. Xie, W. Yang, *Sci. Adv.* **2017**, *3* e1602045.
[9] B. T. Phillips, K. P. Becker, S. Kurumaya, K. C. Galloway, G. Whittredge, D. M. Vogt, C. B. Teeple, M. H. Rosen, V. A. Pieribone, D. F. Gruber, R. J. Wood, *Sci. Rep.* **2018**, *8*, 14779.
[10] S. M. Youssef, M. Soliman, M. A. Saleh, M. A. Mousa, M. Elsamanty, A. G. Radwan, *Micromachines* **2022**, *13*, 110.
[11] G. Li, X. Chen, F. Zhou, Y. Liang, Y. Xiao, X. Cao, Z. Zhang, M. Zhang, B. Wu, S. Yin, Y. Xu, H. Fan, Z. Chen, W. Song, W. Yang, B. Pan, J. Hou, W. Zou, S. He, X. Yang, G. Mao, Z. Jia, H. Zhou, T. Li, S. Qu, Z. Xu, Z. Huang, Y. Luo, T. Xie, J. Gu, et al. *Nature* **2021**, *591*, 66.
[12] K. C. Galloway, K. P. Becker, B. Phillips, J. Kirby, S. Licht, D. Tchernov, R. J. Wood, D. F. Gruber, *Soft Robot.* **2016**, *3*, 23.
[13] S. Kurumaya, B. T. Phillips, K. P. Becker, M. H. Rosen, D. F. Gruber, K. C. Galloway, K. Suzumori, R. J. Wood, *Soft Robot.* **2018**, *5*, 399.
[14] D. M. Vogt, K. P. Becker, B. T. Phillips, M. A. Graule, R. D. Rotjan, T. M. Shank, E. E. Cordes, R. J. Wood, D. F. Gruber, *PLoS ONE* **2018**, *13*, e0200386.
[15] O. V. Zaitseva, *Neurosci. Behav. Physiol.* **1994**, *24*, 47.
[16] N. Krajcs, L. Hernádi, K. Elekes, S. Kimura, T. Kiss, *Invert. Neurosci.* **2014**, *14*, 59.
[17] N. Krajcs, L. Márk, K. Elekes, T. Kiss, *Acta Biol. Hung.* **2012**, *63*, 129.
[18] L. Hernádi, T. Teyke, *Cell Tissue Res.* **2013**, *352*, 217.
[19] B. T. Phillips, S. Licht, K. S. Haiat, J. Bonney, J. Allder, N. Chaloux, R. Shomberg, T. J. Noyes, *Deep Sea Res., Part I* **2019**, *153*, 103136.
[20] Y. Haga, Y. Tanahashi, M. Esashi, in *Proc. MEMS 98. IEEE. Eleventh Annual Inter. Workshop on Micro Electro Mechanical Systems. An Investigation of Micro Structures, Sensors, Actuators, Machines and Systems (Cat. No.98CH36176)*, IEEE, Piscataway, NJ, **1998**, pp. 419–424.
[21] B. He, K. Yang, in *2009 Int. Conf. on Electrical Machines and Systems*, IEEE, Piscataway, NJ **2009**, pp. 1–4.
[22] H. Yang, M. Xu, W. Li, S. Zhang, *IEEE Trans. Ind. Electron.* **2019**, *66*, 6108.
[23] J. Mohd Jani, M. Leary, A. Subic, M. A. Gibson, *Mater. Des.* **2014**, *56*, 1078.
[24] M. W. Hannan, I. D. Walker, *J. Robot. Syst.* **2003**, *20*, 45.
[25] Y. Zhang, M. Su, M. Li, R. Xie, H. Zhu, Y. Guan, in *2017 IEEE Int. Conf. on Mechatronics and Automation (ICMA)*, IEEE, Piscataway, NJ **2017**, pp. 677–682.
[26] A. Y. Yousef, S. M. Abdelmaksoud, *Int. J. Res. Emerg. Sci. Technol.* **2015**, *2*, 5.
[27] X. An, Y. Cui, H. Sun, Q. Shao, H. Zhao, *IEEE Trans. Robot.* **2023**, *39*, 2325.
[28] L. Nagua, C. Relaño, C. A. Monje, C. Balaguer, *Mathematics* **2021**, *9*, 1468.
[29] E. Jones Parry, D. Tabor, *J. Mater. Sci.* **1973**, *8*, 1510.
[30] M. Paterson, *J. Appl. Phys.* **1964**, *35*, 176.